nature neuroscience

Hippocampo-cortical coupling mediates memory consolidation during sleep

Nicolas Maingret[1–4], Gabrielle Girardeau[1–6], Ralitsa Todorova[1–4,6], Marie Goutierre[1–4] & Michaël Zugaro[1–4]

Memory consolidation is thought to involve a hippocampo-cortical dialog during sleep to stabilize labile memory traces for long-term storage. However, direct evidence supporting this hypothesis is lacking. We dynamically manipulated the temporal coordination between the two structures during sleep following training on a spatial memory task specifically designed to trigger encoding, but not memory consolidation. Reinforcing the endogenous coordination between hippocampal sharp wave-ripples, cortical delta waves and spindles by timed electrical stimulation resulted in a reorganization of prefrontal cortical networks, along with subsequent increased prefrontal responsivity to the task and high recall performance on the next day, contrary to control rats, which performed at chance levels. Our results provide, to the best of our knowledge, the first direct evidence for a causal role of a hippocampo-cortical dialog during sleep in memory consolidation, and indicate that the underlying mechanism involves a fine-tuned coordination between sharp wave-ripples, delta waves and spindles.

The 'two-stage' theory of memory posits that memory consolidation involves a dialog during sleep between the hippocampus, where traces are initially formed, and the neocortex, where they are stored for long-term retention[1,2]. Candidate target neocortical areas include the medial prefrontal cortex (mPFC), which receives monosynaptic input from the hippocampus[3]. Over the course of days, the mPFC becomes progressively involved in spatial memory recall, concomitantly with a gradual hippocampal disengagement[4,5]. Consistent with the hypothesized dialog during sleep, task-related neural activity patterns are replayed during sleep, both in the hippocampus[6,7] and mPFC[8,9]. Coordination between the two structures could involve various oscillations that are known to have a causal role in memory consolidation. These include hippocampal sharp wave-ripples (SPW-Rs)[10,11] (150–200 Hz), cortical slow oscillations[12,13] and delta waves[14] (0.1–4 Hz), and thalamo-cortical spindles[15] (10–20 Hz), which are often observed in temporal proximity[16–20]. However, the causal role of a hippocampo-cortical dialog in memory consolidation has remained speculative.

To provide direct evidence for this hypothesis, we first characterized the endogenous temporal coordination between brain oscillations in the hippocampus and mPFC during slow-wave sleep (SWS). The observed coupling selectively increased following training on a task leading to memory consolidation, but not following time-limited training on the same task that did not result in memory consolidation. We then boosted this coupling during sleep following time-limited training by applying SPW-R–triggered stimulation to the neocortex, which induced propagating delta waves and spindles. This resulted in the reorganization of activity profiles in selected mPFC neurons, as well as a subsequent increase in prefrontal responsivity to the task and high recall performance on the next day, in contrast with control rats, which performed at chance levels.

RESULTS

Hippocampo-cortical oscillatory coupling

The hippocampal network is most active during SPW-Rs[2]. We therefore examined the temporal correlation between SPW-Rs in the hippocampus and cortical delta waves and spindles in the mPFC during unperturbed SWS in rats. Delta waves reflect the down states of the slow oscillation[21,22], when cortical neurons stop firing (**Fig. 1a**). Consistent with previous reports[16–18], delta waves were prevalent in close temporal proximity to hippocampal SPW-Rs, with probability peaking at ~130 ms after SPW-Rs (**Fig. 1b** and **Supplementary Fig. 1a**), indicating that delta waves generally followed SPW-Rs. A lower and broader peak ~140 ms before SPW-Rs further indicated that delta waves were, in turn, often followed by SPW-Rs, although this pattern was more temporally diffuse. In most cases, spindles closely followed a delta wave[18,23] (**Supplementary Fig. 1b**). Consistently, delta-spindle sequences were most probable ~140 ms after SPW-Rs (**Fig. 1b**). Thus, we hypothesized that the fine temporal relation between SPW-Rs and delta-spindle sequences is instrumental for communication between the hippocampus and neocortex.

Consolidation-associated increase in oscillatory coupling

A straightforward consequence of our hypothesis is that this coupling should increase when learning leads to memory consolidation. We therefore measured the incidence of coupled SPW-Rs and delta-spindle sequences following training on a hippocampus-dependent memory task[24] (**Fig. 1c**). In the encoding phase, rats were exposed to two identical objects that were located in adjacent corners of a rectangular box for either 3 min (time-limited training) or 20 min (complete training). In the recall phase on the following day, one of the objects was moved to a different corner before the rats were allowed to visit the rectangular box. As previously reported[25], only complete training yielded memory

[1]Collège de France, Center for Interdisciplinary Research in Biology (CIRB), Paris, France. [2]CNRS UMR 7241, Paris, France. [3]INSERM U1050, Paris, France. [4]PSL Research University, Paris, France. [5]Present address: Neuroscience Institute, New York University Medical Center, New York, New York, USA. [6]These authors contributed equally to this work. Correspondence should be addressed to M.Z. (michael.zugaro@college-de-france.fr).

Received 18 December 2015; accepted 14 April 2016; published online 16 May 2016; doi:10.1038/nn.4304

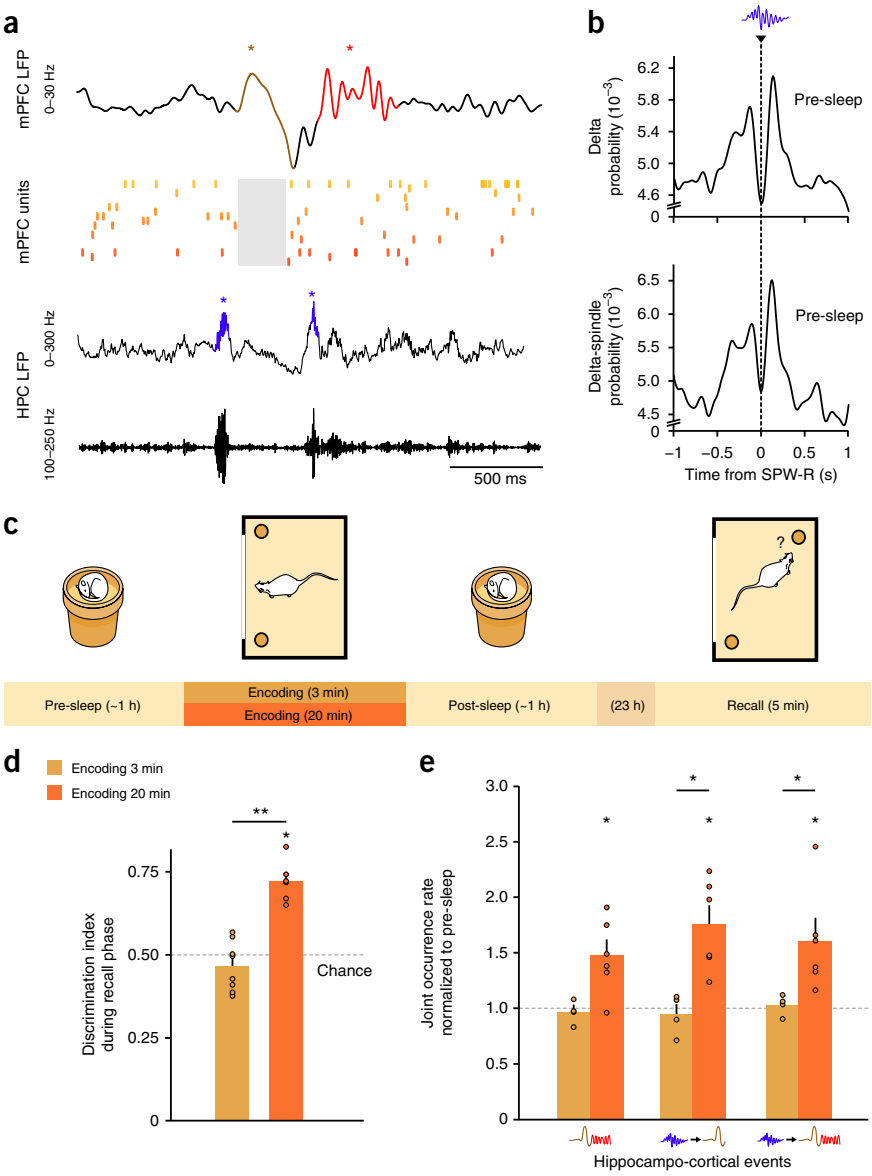

Figure 1 Increased hippocampo-cortical oscillatory coupling correlates with memory consolidation. (**a**) Example traces of LFPs recorded in the mPFC (top trace, low-pass filtered) and hippocampus (center trace, low-pass filtered; bottom trace, filtered in the ripple band) during a typical sleep session. Raster plots show action potentials (colored vertical ticks) emitted by individual prefrontal units. SPW-Rs (blue traces and asterisks), delta waves (brown traces and asterisk) and spindles (red traces and asterisk) are highlighted for clarity. Note the mPFC neuronal silence during delta waves (down states, gray shading). (**b**) Temporal cross-correlation between SPW-Rs and delta waves (top) or delta-spindle sequences (bottom) during SWS preceding a behavioral task (pre-sleep, $n = 7$ animals). Note the temporal proximity between these patterns. (**c**) The rats were allowed to explore the arena and encode the locations of the two objects for either 3 or 20 min. Pre- and post-encoding sleep recordings were carried out in both conditions. (**d**) Discrimination indices during the recall phase, computed during the first 2 min of exploration. The rats discriminated between the stable and displaced objects only after the 20-min encoding phase (3 versus 20 min encoding, Wilcoxon rank-sum test, $n = 8$, $n = 6$, $Z = 3.00$, $^{**}P = 0.002$; 3 min versus chance, Wilcoxon signed-rank test, $n = 8$, $Z = 1.40$, $P = 0.161$; 20 min versus chance, Wilcoxon signed-rank test, $n = 6$, $Z = 2.20$, $^{*}P = 0.028$). (**e**) Incidence of hippocampo-cortical events during SWS following either 3- (ochre) or 20-min (orange) encoding (left, delta spindle; center: SPW-R–delta; right, SPW-R–delta spindle), normalized to corresponding pre-sleep epochs. Note the increase in hippocampo-cortical event rate following the 20-min, but not 3-min, exposure to the objects. Delta-spindle incidence, 3 min versus 20 min encoding, Wilcoxon rank-sum test, $n = 4$, $n = 6$, $Z = 1.81$, $P = 0.067$; 3 min versus chance, Wilcoxon signed-rank test, $n = 4$, $Z = 0.73$, $P = 0.465$; 20 min versus chance, Wilcoxon signed-rank test, $n = 6$, $Z = 1.99$, $^{*}P = 0.046$. SPW-R–delta incidence, 3 min versus 20 min encoding, Wilcoxon rank-sum test, $n = 4$, $n = 6$, $Z = 2.45$, $^{*}P = 0.014$; 3 min versus chance, Wilcoxon signed-rank test, $n = 4$, $Z = 0.36$, $P = 0.715$; 20 min versus chance, Wilcoxon signed-rank test, $n = 6$, $Z = 2.20$, $^{*}P = 0.028$. SPW-R–delta-spindle incidence, 3 min versus 20 min encoding, Wilcoxon rank-sum test, $n = 4$, $n = 6$, $Z = 2.45$, $^{*}P = 0.014$; 3 min versus chance, Wilcoxon signed-rank test, $n = 4$, $Z = 0.73$, $P = 0.465$; 20 min versus chance, Wilcoxon signed-rank test, $n = 6$, $Z = 2.20$, $^{*}P = 0.028$. Error bars represent s.e.m.

consolidation 24 h later, as measured by preferential exploration of the displaced object (discrimination indices: time-limited training, 0.45 ± 0.04; complete training, 0.72 ± 0.03; **Fig. 1d** and **Supplementary Table 1**). Consistent with our prediction, enhanced hippocampo-cortical coupling co-occurred with memory consolidation, as joint occurrence of hippocampal and cortical rhythms selectively increased after complete, but not time-limited, training (**Fig. 1e**).

Causal role of the hippocampo-cortical dialog

To establish a causal link between increased hippocampo-cortical coupling and memory consolidation, we designed a closed-loop stimulation protocol to dynamically and selectively enhance the temporal coupling between SPW-Rs and delta spindles during SWS. SPW-Rs were detected online by band-pass filtering (100–250 Hz) and thresholding the hippocampal local field potential (LFP)[10]. Threshold crossing automatically triggered brief (0.1 ms, 20 V) single-pulse stimulation of the neocortex, evoking propagating delta waves followed by spindles[26]. To avoid hyper-synchronous recruitment of the mPFC network by direct current injection and to ensure that delta waves and spindles would be elicited at the optimal delay, emulating endogenous events in the mPFC, we targeted the stimulation to the deep layers of the motor cortex. Delta waves would subsequently propagate across the cortical mantle[26], including the mPFC. This protocol resulted in a dynamic, temporally specific reinforcement of the endogenous coupling between SPW-Rs and delta spindles (**Fig. 2a–c**).

To test the effect of increased coupling between SPW-Rs and delta spindles on memory consolidation, we trained rats ($n = 9$) on the time-limited (3 min) version of the task. Our goal was to potentiate the consolidation of the weak memory traces by reinforcing the hippocampo-cortical oscillatory interactions during SWS following

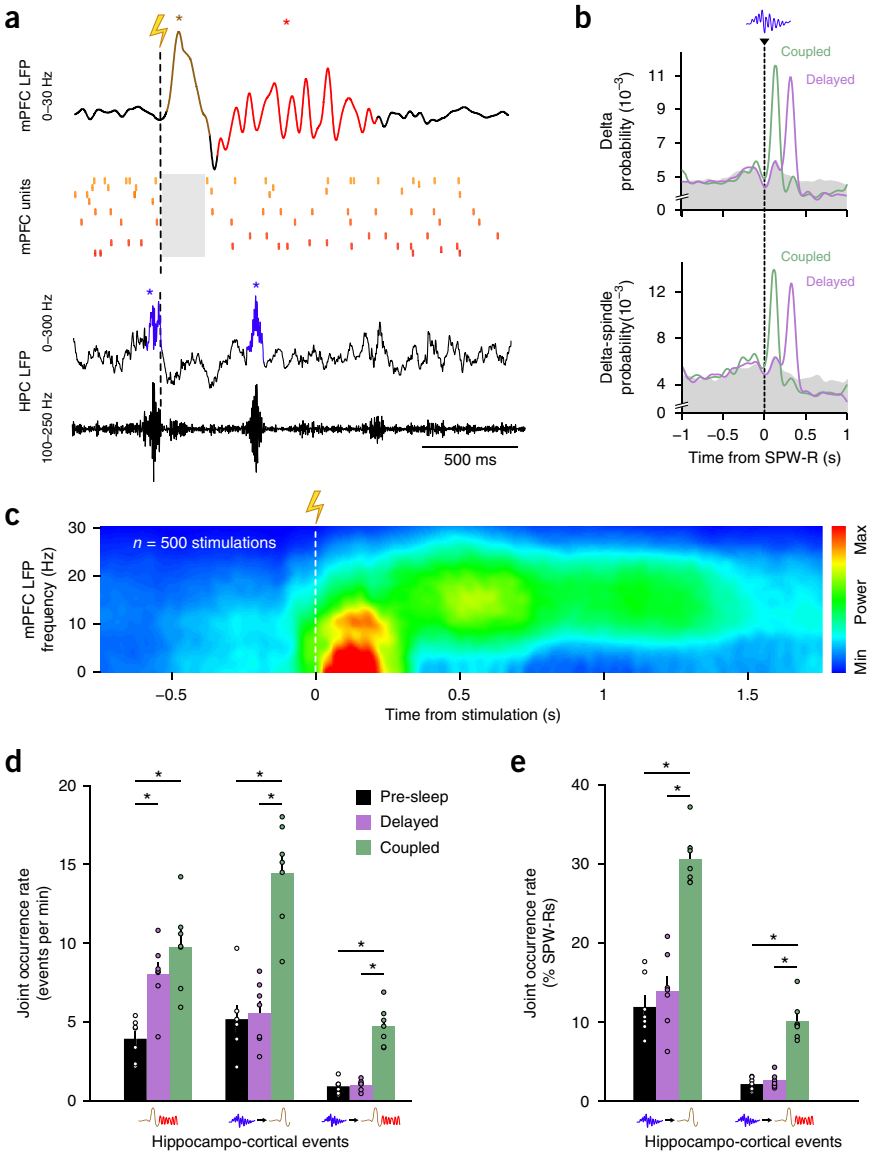

Figure 2 SPW-R–triggered stimulation of neocortical deep layers enhances the temporal coupling between hippocampal and cortical events. (**a**) Example SPW-R–triggered stimulation of neocortical deep layers (lightning icon and vertical dotted line), which induced a delta wave followed by a spindle in the mPFC, similar to the endogenous pattern observed in **Figure 1a**. (**b**) Data presented as in **Figure 1b**, but during SWS periods when stimulation was triggered following SPW-R detection (green curves) or following a brief (160–240 ms) pseudo-random delay (purple curves). Pre-sleep values from **Figure 1b** are shown in gray ($n = 7$ animals). (**c**) Stimulation-triggered average spectrogram of mPFC LFPs for a coupled stimulation session in one rat. Note the marked increase in delta power (0–6 Hz), followed by spindle activity (10–20 Hz). (**d**) Incidence of hippocampo-cortical events (left, delta spindle; center, SPW-R–delta; right: SPW-R–delta spindle) during pre-sleep (black) and stimulation periods (purple, delayed stimulation; green, coupled stimulation). Delta-spindle incidence, Friedman test, $\chi^2 = 10.57$, $n = 7$, d.f. = 2, $P = 0.005$; Wilcoxon matched pairs test, $n = 7$, pre-sleep versus coupled: $Z = 2.36$, $^*P = 0.018$; pre-sleep versus delayed: $Z = 2.36$, $^*P = 0.018$; coupled versus delayed: $Z = 1.18$, $P = 0.237$. SPW-R–delta incidence, Friedman test, $\chi^2 = 10.57$, $n = 7$, d.f. = 2, $P = 0.005$; Wilcoxon matched pairs test, $n = 7$, pre-sleep versus coupled: $Z = 2.36$, $^*P = 0.018$; pre-sleep versus delayed: $Z = 0.68$, $P = 0.499$; coupled versus delayed: $Z = 2.36$, $^*P = 0.018$. SPW-R–delta-spindle incidence, Friedman test, $\chi^2 = 11.14$, $n = 7$, *d.f.* = 2, $P = 0.004$; Wilcoxon matched pairs test, $n = 7$, pre-sleep versus coupled: $Z = 2.36$, $^*P = 0.018$; pre-sleep versus delayed: $Z = 1.69$, $P = 0.091$; coupled versus delayed: $Z = 2.36$, $^*P = 0.018$. (**e**) Data presented as in **d**, but expressed as a proportion of SPW-Rs. SPW-R–delta percentage, Friedman test, $\chi^2 = 11.14$, $n = 7$, *d.f.* = 2, $P = 0.004$; Wilcoxon matched pairs test, $n = 7$, pre-sleep versus coupled: $Z = 2.36$, $^*P = 0.018$; pre-sleep versus delayed: $Z = 1.86$, $P = 0.063$; coupled versus delayed: $Z = 2.36$, $^*P = 0.018$. SPW-R–delta spindle percentage, Friedman test, $\chi^2 = 11.14$, $n = 7$, *d.f.* = 2, $P = 0.004$; Wilcoxon matched pairs test, $n = 7$, pre-sleep versus coupled: $Z = 2.36$, $^*P = 0.018$; pre-sleep versus delayed: $Z = 1.69$, $P = 0.091$; coupled versus delayed: $Z = 2.36$, $^*P = 0.018$. Error bars represent s.e.m.

encoding. In the coupled stimulation condition, stimulations (n = 1,000) were triggered following SPW-R detection to reinforce the coordination between SPW-Rs and delta spindles. In the delayed stimulation condition, the stimulations (n = 1,000) were delayed by a random interval (160–240 ms) to probe the functional specificity of a fine-tuned temporal sequence between hippocampal and neocortical events. The same animals were used in both conditions: each rat performed the task twice (using different object pairs), once for each stimulation protocol (coupled and delayed), in a pseudo-randomized order. In both cases, the period of stimulation corresponded to the first ~4,000 s of SWS following the encoding phase, when most hippocampal replay events were expected to occur[27].

Stimulations reliably induced delta waves (stimulation efficacy: coupled, 66.5 ± 3.3%; delayed, 65.2 ± 4.8%) and spindles (stimulation efficacy: coupled, 39.8 ± 4.0%; delayed, 41.0 ± 4.2%). Notably, stimulation efficacy was identical in the two stimulation protocols (**Supplementary Fig. 2a**). As a result, although the incidence of SPW-Rs was not affected by the stimulation (**Supplementary Fig. 2b**), the overall occurrence rates of both delta waves and spindles were higher during stimulation periods than during baseline sleep, but were identical in the two stimulation protocols (**Supplementary Fig. 2b**). Moreover, delta waves and spindles had unaltered peak power across conditions (**Supplementary Fig. 2c,d**). Induced delta waves were associated with a near-complete cessation of mPFC spiking activity (down state; **Fig. 2a** and **Supplementary Fig. 2e**) and did not differentially affect hippocampal firing rates (**Supplementary Fig. 2f**). Stimulations did not directly drive spiking activity in the mPFC (**Supplementary Fig. 3**), nor did the two stimulation conditions differentially alter the global sleep architecture (**Supplementary Fig. 4**).

As expected, coupled stimulations strongly enhanced the temporal correlation between hippocampal and cortical oscillations (**Fig. 2b,c** and Online Methods). Delta-spindle sequences were elicited ~120 ms after SPW-Rs, emulating endogenous patterns observed in baseline sleep, but the incidence of SPW-R–delta-spindle sequences was

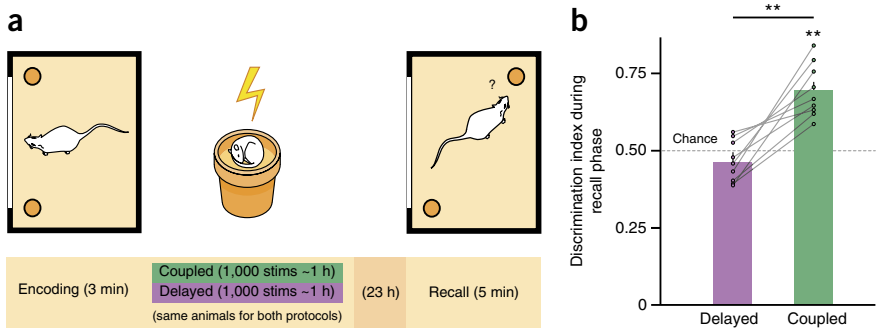

Figure 3 Enhancing the fine-tuned coupling of hippocampal SPW-Rs and cortical delta waves and spindles boosts next day performance in a spatial memory task. (**a**) Rats ($n = 9$) were exposed for 3 min to two identical objects located in two adjacent corners of a familiar arena (encoding phase) and then underwent SPW-R–triggered cortical stimulation ($n = 1{,}000$) during SWS following the task (~1 h). Each animal performed the task twice (with different object pairs), in pseudo-random order. In the coupled condition, stimulation was delivered following SPW-R detection. In the delayed condition, stimulation occurred after a random delay (160–240 ms) following SPW-R detection. Twenty-four hours after the encoding phase, one of the objects was displaced to the opposite corner, and the animals were allowed to explore the arena for 5 min (recall phase). Memory recall was reflected in a preferential exploration of the displaced object. Note that in the absence of stimulation following the encoding phase, non-implanted control animals performed at chance level the following day ($n = 8$; **Fig. 1d**). (**b**) Discrimination index for the displaced object during the recall phase, computed during the first 2 min of exploration. Memory recall was observed only following coupled stimulation (coupled versus delayed, Wilcoxon matched pairs test, $n = 9$, $Z = 2.67$, $^{**}P = 0.008$; coupled versus chance, Wilcoxon signed-rank test, $n = 9$, $Z = 2.67$, $^{**}P = 0.008$; delayed versus chance, Wilcoxon signed-rank test, $n = 9$, $Z = 1.48$, $P = 0.139$). Error bars represent s.e.m.

increased fivefold (**Fig. 2d**). The proportion of SPW-Rs followed by cortical patterns increased by a similar magnitude (**Fig. 2e**). In contrast, delayed stimulation evoked cortical delta waves at latencies of ~320 ms following hippocampal SPW-Rs (**Fig. 2b**), far exceeding the timing of endogenous SPW-R-delta pairs (~130 ms). As a result, joint hippocampo-cortical patterns were unchanged compared with baseline, both in incidence (**Fig. 2d**) and in proportion of SPW-Rs (**Fig. 2e**). Notably, the proportion of induced delta waves followed by SPW-Rs in the two conditions was unchanged compared with endogenous events (**Supplementary Fig. 5**).

How did this selective enhancement of hippocampo-cortical coupling during sleep affect memory consolidation? In the absence of stimulation, performance was not significantly different from chance, that is, the animals spent as much time exploring the stable object as the displaced object (**Fig. 1d**). However, following coupled stimulation, the rats preferentially explored the displaced object (discrimination index, 0.69 ± 0.03; **Fig. 3** and **Supplementary Table 1**), indicating that timed enhancement of the hippocampo-cortical dialog resulted in successful consolidation of the weak memory traces. This bias persisted after 3 or 5 min of exploration (**Supplementary Fig. 6**). Conversely, delayed stimulations did not improve performance above chance level (discrimination index, 0.46 ± 0.04; **Fig. 3** and **Supplementary Table 1**), indicating that fine-tuned temporal coordination between the two structures is required to promote memory consolidation, and ruling out the possibility that the improved performance following coupled stimulation could be accounted for by a mere increase in delta and spindle rates alone. This was further supported by the complementary finding that randomly timed stimulation, unrelated to (that is, uniformly distributed relative to) SPW-R times, also resulted in subsequent chance performance (random stimulation group, discrimination index, 0.48 ± 0.03; **Supplementary Fig. 7** and **Supplementary Table 1**).

Reorganization of the mPFC network

Systems consolidation has been hypothesized to involve reorganization of functional cortical networks[28]. We carried out large-scale unit recordings in stimulated rats and compared spatio-temporal spiking patterns of mPFC pyramidal neurons following coupled versus delayed induced delta waves. First, to examine potential changes in the sequential spread of activity in local cortical networks, we measured cell-specific activation latencies following up-state transitions[29], when cortical activity resumes following silencing during the delta wave. Because latencies are independent of single-cell or global properties, such as excitability or traveling wave direction, and instead appear to reflect local functional connectivity[29], changes in latencies would reflect non-trivial network alterations that are possibly related to consolidation processes. Thus, for each cell, we computed the difference in latency following induced versus endogenous delta waves. Comparison of coupled and delayed stimulation revealed that the latencies of mPFC neurons changed following SPW-R–coupled, but not delayed, delta waves (**Fig. 4a**), suggesting that specific reorganization processes result from hippocampo-cortical interactions. To further investigate selective reshaping of network activity, we then assessed changes in spike train profiles after up state onsets, reflected in the peri-event time histograms (PETHs) of mPFC pyramidal neurons. PETHs were computed for each neuron (**Fig. 4b**,**c**) and compared between coupled and delayed stimulation using a similarity index (uniqueness)[29]. PETHs remained unchanged following delayed stimulation, indicating that mere stimulation did not alter cell-specific features of mPFC spike trains. However, induced delta waves, when coupled to SPW-Rs, gave way to two clearly distinct responses, including stable and varying PETHs (**Fig. 4b**,**c**). This suggests that a specific subpopulation of mPFC cells selectively changed their activity profiles following induced hippocampo-cortical coupling. This was further supported by the finding that, in contrast with the rest of the population, these cells changed the order in which they activated following SPW-R–coupled delta waves (**Fig. 4c**). Finally, to test whether activity changes during sleep were subsequently reflected during recall, we computed an object responsivity index for each mPFC cell and compared the distributions of responsivity indices for each object following coupled versus delayed stimulation sleep sessions. Although mPFC cells did not respond to either object following delayed stimulation sessions, responsivity to the displaced object selectively increased following coupled stimulation sessions, paralleling the improvement in memory recall (**Fig. 4d** and **Supplementary Fig. 8**).

DISCUSSION

Dynamically enhancing the coupling between hippocampal SPW-Rs and cortical delta waves and spindles during SWS resulted in the consolidation of a labile memory trace. Furthermore, this coupling required very fine temporal precision, as introducing a random delay as brief as 200 ms between hippocampal and cortical events was sufficient to cancel the induction of memory consolidation. Our results

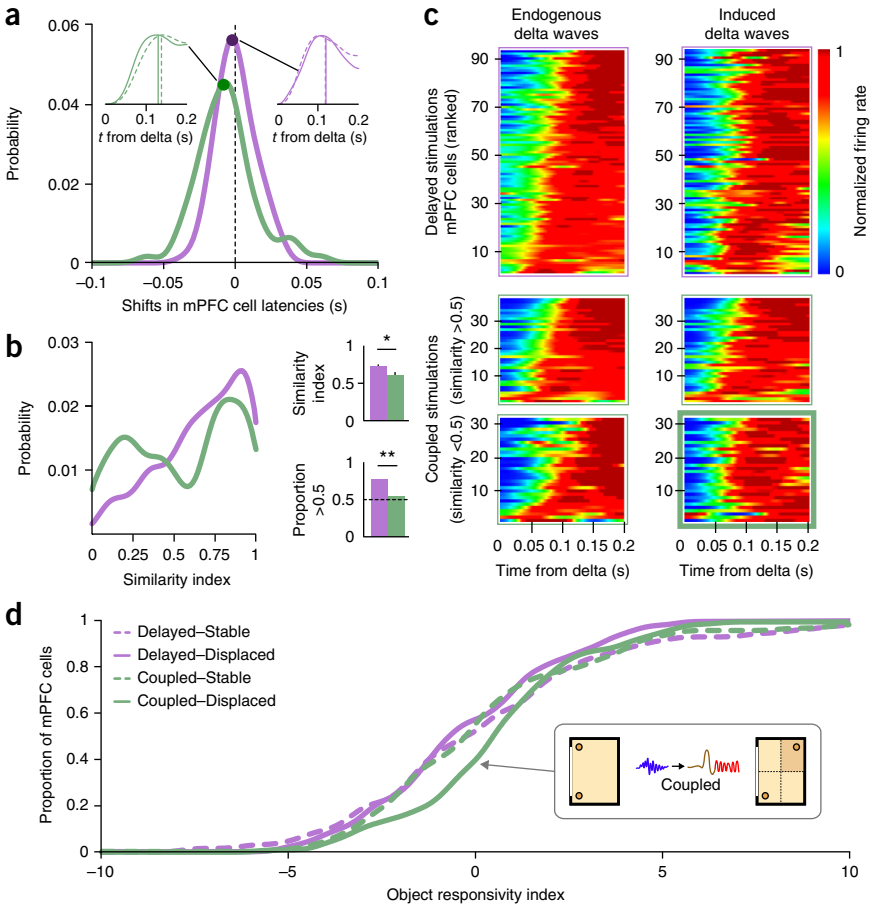

Figure 4 Changes in spatio-temporal spiking profiles of mPFC neurons parallel memory consolidation and recall improvements. (**a**) Distribution of shifts in mPFC cell latencies in stimulation-induced delta waves relative to endogenous, non-SPW-R–coupled delta waves in the coupled (green) and delayed stimulation (purple) sessions. The latencies shifted to more negative values in the coupled condition, indicating changes in the spread of activity in local cortical networks (coupled versus delayed, Wilcoxon rank-sum test, $n = 70$, $n = 93$, $Z = 3.00$, $P = 0.003$; coupled versus zero, Wilcoxon matched pairs test, $n = 70$, $Z = 2.85$, $P = 0.004$; delayed versus zero, Wilcoxon matched pairs test, $n = 93$, $Z = 0.20$, $P = 0.845$). Insets show the PETHs of two typical mPFC cells and the location of their latency differences on the distribution curves. Continuous curves and lines indicate induced up states. Dashed curves and lines indicate endogenous up states. Vertical lines represent mean latencies. (**b**) Distribution of PETH similarity indices (Online Methods) in both stimulation conditions. Bar plots on the right show median similarity indices (coupled versus delayed, Wilcoxon rank-sum test, $n = 70$, $n = 93$, $Z = 2.12$, $^*P = 0.034$) and proportion of cells with a similarity index > 0.5 (two-proportion Z-test, $Z = 3.12$, $^{**}P = 0.001$). The PETH similarity index distribution was bimodal in the coupled condition (Hartigan's dip test, dip = 0.025, $P = 0.0002$), but not in the delayed condition (Hartigan's dip test, dip = 0.006, $P = 0.999$), indicating that a specific subpopulation of mPFC cells selectively changed their activity profiles following induced SPW-R–delta sequences. (**c**) Up state–triggered PETHs for all cells following endogenous (left) and induced (right) delta waves (top, delayed condition; bottom, coupled condition). Individual PETHs are ordered according to their mean latency following endogenous events. Top, delayed condition; note the consistency of cell organization in endogenous and induced events (Spearman's rank correlation, $\rho = 0.668$, $P < 0.001$). Bottom, PETHs are shown separately for mPFC cells in the two subpopulations forming the bimodal distribution in **b** (green). Note the reorganization in the subpopulation with low (<0.5) (Spearman's rank correlation, $\rho = 0.001$, $P = 0.995$), but not high (>0.5), PETH similarity (Spearman's rank correlation, $\rho = 0.854$, $P < 0.001$). (**d**) Cumulative distributions of mPFC responsivity indices for each object during the recall phase of the task following both stimulation protocols. Medial prefrontal cortical cells selectively became responsive to the displaced object following coupled stimulations (displaced object: coupled versus delayed, Wilcoxon rank-sum test, $n = 99$, $n = 61$, $Z = 2.41$, $P = 0.016$; coupled versus zero, Wilcoxon signed-rank test, $n = 99$, $Z = 2.32$, $P = 0.020$; delayed versus zero, Wilcoxon signed-rank test, $n = 61$, $Z = 1.21$, $P = 0.226$; stable object: coupled versus delayed, Wilcoxon rank-sum test, $n = 99$, $n = 61$, $Z = 0.21$, $P = 0.838$; coupled versus zero, Wilcoxon signed-rank test, $n = 99$, $Z = 0.45$, $P = 0.655$; delayed versus zero, Wilcoxon signed-rank test, $n = 61$, $Z = 0.31$, $P = 0.755$). Error bars represent s.e.m.

show that long-term stabilization of memory traces is promoted by timed functional interactions between the hippocampus and cortex during offline states.

The underlying mechanism is a fine-tuned coupling between hippocampal SPW-Rs and cortical delta waves and spindles, orchestrating local network reorganizations in selected subpopulations of mPFC neurons[2,30]. Given that delta waves and spindles are propagating patterns that affect the entire neocortex[26], other cortical areas, including rhinal cortices, may undergo similar reorganization processes.

Following SPW-R–associated replay[6,7,27], cell assemblies would be reactivated in the mPFC[9]. The following cortical delta wave would then isolate target synapses from competing inputs, allowing selective reorganization of the network during the ensuing up state transition and strengthening by subsequent spindles[31]. Depending on learning requirements, cortical patterns could in turn regulate hippocampal SPW-Rs[32].

METHODS

Methods and any associated references are available in the online version of the paper.

Note: Any Supplementary Information and Source Data files are available in the online version of the paper.

ACKNOWLEDGMENTS

We thank C. Drieu, V. Oberto, H.-Y. Gao, A. Cei, S. Sara, S.I. Wiener and K. Benchenane for advice and comments on the manuscript, and S. Doutremer, M.A. Thomas and Y. Dupraz for technical support. This work was supported by the French Ministry of Research (N.M.), a grant from the Fondation pour la Recherche Médicale (grant no. FDT20150532568) (N.M.), and a joint grant from École des Neurosciences de Paris Île-de-France and LabEx MemoLife (ANR-10-LABX-54 MEMO LIFE, ANR-10-IDEX-0001-02 PSL*) (R.T.).

AUTHOR CONTRIBUTIONS

N.M., G.G. and M.Z. designed the study. N.M., G.G. and M.G. performed the experiments. N.M., R.T. and M.Z. designed the analyses. N.M. and R.T. performed the analyses. N.M. and M.Z. wrote the manuscript with input from all authors.

COMPETING FINANCIAL INTERESTS

The authors declare no competing financial interests.

1. Marr, D. Simple memory: a theory for archicortex. *Philos. Trans. R. Soc. Lond. B Biol. Sci.* **262**, 23–81 (1971).
2. Buzsáki, G. Two-stage model of memory trace formation: a role for "noisy" brain states. *Neuroscience* **31**, 551–570 (1989).
3. Ferino, F., Thierry, A.M. & Glowinski, J. Anatomical and electrophysiological evidence for a direct projection from Ammon's horn to the medial prefrontal cortex in the rat. *Exp. Brain Res.* **65**, 421–426 (1987).
4. Maviel, T., Durkin, T.P., Menzaghi, F. & Bontempi, B. Sites of neocortical reorganization critical for remote spatial memory. *Science* **305**, 96–99 (2004).
5. Bontempi, B., Laurent-Demir, C., Destrade, C. & Jaffard, R. Time-dependent reorganization of brain circuitry underlying long-term memory storage. *Nature* **400**, 671–675 (1999).
6. Wilson, M.A. & McNaughton, B.L. Reactivation of hippocampal ensemble memories during sleep. *Science* **265**, 676–679 (1994).
7. Lee, A.K. & Wilson, M.A. Memory of sequential experience in the hippocampus during slow-wave sleep. *Neuron* **36**, 1183–1194 (2002).
8. Euston, D.R., Tatsuno, M. & McNaughton, B.L. Fast-forward playback of recent memory sequences in prefrontal cortex during sleep. *Science* **318**, 1147–1150 (2007).
9. Peyrache, A., Khamassi, M., Benchenane, K., Wiener, S.I. & Battaglia, F.P. Replay of rule-learning related neural patterns in the prefrontal cortex during sleep. *Nat. Neurosci.* **12**, 919–926 (2009).
10. Girardeau, G., Benchenane, K., Wiener, S.I., Buzsáki, G. & Zugaro, M.B. Selective suppression of hippocampal ripples impairs spatial memory. *Nat. Neurosci.* **12**, 1222–1223 (2009).
11. Ego-Stengel, V. & Wilson, M.A. Disruption of ripple-associated hippocampal activity during rest impairs spatial learning in the rat. *Hippocampus* **20**, 1–10 (2010).
12. Marshall, L., Helgadóttir, H., Mölle, M. & Born, J. Boosting slow oscillations during sleep potentiates memory. *Nature* **444**, 610–613 (2006).
13. Ngo, H.-V.V., Martinetz, T., Born, J. & Mölle, M. Auditory closed-loop stimulation of the sleep slow oscillation enhances memory. *Neuron* **78**, 545–553 (2013).
14. Johnson, L.A., Euston, D.R., Tatsuno, M. & McNaughton, B.L. Stored-trace reactivation in rat prefrontal cortex is correlated with down-to-up state fluctuation density. *J. Neurosci.* **30**, 2650–2661 (2010).
15. Mednick, S.C. *et al.* The critical role of sleep spindles in hippocampal-dependent memory: a pharmacology study. *J. Neurosci.* **33**, 4494–4504 (2013).
16. Sirota, A., Csicsvari, J., Buhl, D. & Buzsáki, G. Communication between neocortex and hippocampus during sleep in rodents. *Proc. Natl. Acad. Sci. USA* **100**, 2065–2069 (2003).
17. Battaglia, F.P., Sutherland, G.R. & McNaughton, B.L. Hippocampal sharp wave bursts coincide with neocortical "up-state" transitions. *Learn. Mem.* **11**, 697–704 (2004).
18. Peyrache, A., Battaglia, F.P. & Destexhe, A. Inhibition recruitment in prefrontal cortex during sleep spindles and gating of hippocampal inputs. *Proc. Natl. Acad. Sci. USA* **108**, 17207–17212 (2011).
19. Phillips, K.G. *et al.* Decoupling of sleep-dependent cortical and hippocampal interactions in a neurodevelopmental model of schizophrenia. *Neuron* **76**, 526–533 (2012).
20. Staresina, B.P. *et al.* Hierarchical nesting of slow oscillations, spindles and ripples in the human hippocampus during sleep. *Nat. Neurosci.* **18**, 1679–1686 (2015).
21. Steriade, M., Nuñez, A. & Amzica, F. A novel slow (<1 Hz) oscillation of neocortical neurons *in vivo*: depolarizing and hyperpolarizing components. *J. Neurosci.* **13**, 3252–3265 (1993).
22. Sirota, A. & Buzsáki, G. Interaction between neocortical and hippocampal networks via slow oscillations. *Thalamus Relat. Syst.* **3**, 245–259 (2005).
23. Amzica, F. & Steriade, M. Cellular substrates and laminar profile of sleep K-complex. *Neuroscience* **82**, 671–686 (1998).
24. Barker, G.R.I. & Warburton, E.C. When is the hippocampus involved in recognition memory? *J. Neurosci.* **31**, 10721–10731 (2011).
25. Ballarini, F., Moncada, D., Martinez, M.C., Alen, N. & Viola, H. Behavioral tagging is a general mechanism of long-term memory formation. *Proc. Natl. Acad. Sci. USA* **106**, 14599–14604 (2009).
26. Vyazovskiy, V.V., Faraguna, U., Cirelli, C. & Tononi, G. Triggering slow waves during NREM sleep in the rat by intracortical electrical stimulation: effects of sleep/wake history and background activity. *J. Neurophysiol.* **101**, 1921–1931 (2009).
27. Kudrimoti, H.S., Barnes, C.A. & McNaughton, B.L. Reactivation of hippocampal cell assemblies: effects of behavioral state, experience, and EEG dynamics. *J. Neurosci.* **19**, 4090–4101 (1999).
28. Frankland, P.W. & Bontempi, B. The organization of recent and remote memories. *Nat. Rev. Neurosci.* **6**, 119–130 (2005).
29. Luczak, A., Barthó, P., Marguet, S.L., Buzsáki, G. & Harris, K.D. Sequential structure of neocortical spontaneous activity in vivo. *Proc. Natl. Acad. Sci. USA* **104**, 347–352 (2007).
30. Womelsdorf, T. *et al.* Modulation of neuronal interactions through neuronal synchronization. *Science* **316**, 1609–1612 (2007).
31. Rosanova, M. & Ulrich, D. Pattern-specific associative long-term potentiation induced by a sleep spindle–related spike train. *J. Neurosci.* **25**, 9398–9405 (2005).
32. Girardeau, G., Cei, A. & Zugaro, M. Learning-induced plasticity regulates hippocampal sharp wave-ripple drive. *J. Neurosci.* **34**, 5176–5183 (2014).

ONLINE METHODS

Animals. All experiments were carried out in accordance with institutional (CNRS Comité Opérationnel pour l'Éthique dans les Sciences de la Vie) and international (US National Institutes of Health guidelines) standards, legal regulations (Certificat no. B751756), and ethical requirements (Ethics Committee approval #2012-0048) regarding the use and care of animals.

A total of 23 male Long Evans rats (René Janvier; weight, 280–350 g) were maintained on a 12-h:12-h light-dark cycle (lights on at 07:00 a.m.). Training and experiments took place during the day. Rats were group-housed until 1 week before surgery.

Surgery. Electrophysiological signals were acquired using tetrodes (groups of four twisted 12-µm tungsten wires, gold-plated to ~200 kΩ). The rats (n = 15) were deeply anesthetized (xylazine, 0.1 ml intramuscular; pentobarbital, 40 mg per kg of body weight, intraperitoneal; 0.1 ml pentobarbital supplemented every hour) and implanted with a custom-built microdrive allowing for the adjustment of up to 16 individual tetrodes. Rats were implanted with 6 (n = 3 rats, **Fig. 1d**,**e**; n = 3 rats, **Supplementary Fig. 7**) or 16 (n = 9 rats, **Figs. 2** and **3**) tetrodes targeted at the prelimbic and infralimbic regions of the right mPFC (AP: +2.7 mm from bregma; ML: +1.5 mm, angled at 10° from the sagittal plane) and the CA1 subfield of the right hippocampus (AP: −3.5 to −5.5 mm; ML: +2.5 to +5 mm). For the animals that underwent stimulation, a custom-built bipolar electrode consisting of two stainless steel wires (total length, 1.5 mm; inter-wire interval, 0.5 mm; wire diameter, 70 µm) was implanted in the contralateral neocortex (AP: +2 mm; ML: −2 mm; DV: −1.5 mm from the dura (motor area); n = 9 rats for coupled and delayed stimulation, n = 3 rats for random stimulation). Miniature stainless steel screws (reference and ground) were implanted above the cerebellum. During recovery from surgery (minimum 3 d), the rats received food and water *ad libitum*. The recording electrodes were then progressively lowered until they reached their targets and then adjusted every day to optimize yield and stability.

Recording and stimulation. All training and recording sessions took place in the same dimly lit room, enclosed by black curtains. Behavior was monitored using an overhead video camera. One red light–emitting diode was fixed on the front of the microdrive to track the position of the animal. For rest and sleep sessions, rats were secluded in a familiar flower pot in the center of the recording arena. All analyses were conducted offline. Brain signals were preamplified (unity-gain headstage, Noted Bt), amplified 500× (Neuralynx L8), acquired and digitized with two synchronized Power1401 systems (CED). During stimulation periods, threshold crossing on the ripple band-filtered hippocampal signal automatically triggered a monophasic single-pulse (0.1 ms) stimulation of the deep layers of the motor cortex, delivered by a constant current stimulator (SD9 square pulse stimulator, Grass Technologies). This induced the initiation and propagation of a delta wave across neocortical areas[26]. For each animal, the optimal stimulation voltage was defined as the minimum voltage necessary to reliably induce propagating delta waves, and was determined before training (range: 17.5–22.5 V). In the test condition (coupled), stimulation was used to emulate the endogenous fine-tuned coordination between hippocampal and cortical rhythms, and were therefore triggered 20 ms after SPW-R detection. In the control condition (delayed), an additional random delay ranging from 160–240 ms was introduced between SPW-R detection and stimulation onset. In both coupled and delayed conditions, the number of stimulations was limited to one every 2 s to ensure that a stimulation would not be triggered before the end of the previous elicited spindle (see **Fig. 2c**), and the total number of stimulations was set to 1,000, yielding a stimulation period of ~4,000 s during which most replay events were expected to occur[27].

Behavioral protocol. All experiments (behavior and sleep sessions) took place in a dimly lit area enclosed by dark curtains. A 70-cm × 50-cm arena with 50-cm-high black plastic walls (**Fig. 1c**) was used for the behavioral task. A white card (20 × 30 cm) on one wall served as a visual reference cue. During the habituation phase, the rats were allowed to freely explore the empty arena for 20 min once a day for 3 consecutive days. The spatial object recognition task consisted of an encoding and a recall phase, separated by a ~24-h interval. Both phases took place at the same time of the day. During the encoding phase, two identical objects were placed in two adjacent corners. The rats were released in the center of the arena and allowed to explore for either 3 min (time-limited training) or 20 min (complete training). Time-limited training was intended to foil recall of the spatial configuration of the objects on the next day[25] (**Fig. 1d**; if the rats expressed a preference for one of the two objects during the encoding phase, the trial was aborted, and the rats were tested again 48 h later with different objects). The rats were then placed in a flower pot for sleep sessions, which lasted until 1,000 stimulations had been delivered (~4,000 s of SWS), then returned to their home cage. The recall phase took place the following day. One of the objects was displaced to the opposite corner and the animals were allowed to freely explore the arena for 5 min. The same rats (n = 9) underwent coupled and delayed stimulation: they performed the task twice (with different objects), in a pseudo-random order, at an interval of at least two days. Rats used for the random stimulation protocol (n = 3) and unimplanted rats used for the complete training protocol (n = 3) also performed the task twice. Data collection and analysis were not performed blind to the conditions of the experiments.

The discrimination index was defined as the time spent exploring the displaced object divided by the total time of exploration of both objects. The rats were considered to be exploring an object whenever their head was oriented toward and located within 2 cm of the object. Exploration time was measured from video files, both automatically and manually by two independent experimenters. All three measures yielded equivalent results (Friedman test, $\chi^2 = 1.56$, n = 9, d.f. = 2, P = 0,459), and the data presented here were derived with the automatic detection algorithm.

Data processing and spike sorting. A red LED was used to track the instantaneous position of animals (recorded at 25 Hz, resampled at 39.0625 Hz). For off-line spike sorting, the wide-band signals were converted, digitally high-pass filtered (nonlinear median-based filter) and thresholded, and waveforms were extracted and projected to a PCA subspace using NDManager (L. Hazan and M.Z., http://neurosuite.sourceforge.net)[33]. Spike sorting used a semi-automatic cluster cutting procedure combining KlustaKwik (K.D. Harris, http://klustakwik.sourceforge.net) and Klusters (L. Hazan, http://neurosuite.sourceforge.net)[33]. Putative interneurons and pyramidal cells were discriminated based on spike width[34]. Neurophysiological and behavioral data were explored using NeuroScope (L. Hazan, http://neurosuite.sourceforge.net)[33]. LFPs were derived from wide-band signals by downsampling all channels to 1,250 Hz.

Data analysis *Statistics.* Data were analyzed using Matlab (Statistical Toolbox; FMAToolbox, M.Z., http://fmatoolbox.sourceforge.net). Spectrograms were constructed using Chronux (http://chronux.org/). No statistical methods were used to pre-determine sample sizes, but our sample sizes are similar to those generally employed in the field. All statistical tests were non-parametric and two-tailed. In accordance with standard procedures, proportional data were transformed as $P' = \arcsin(\sqrt{P})$, before performing non-parametric (for example, Wilcoxon matched pairs or Friedman) tests.

SPW-Rs, delta waves and spindles. For offline SPW-R detection, the LFP recorded in CA1 pyramidal layer was band-pass filtered (150–250 Hz), squared, low-pass filtered (8.8 ms running average) and normalized, yielding a transformed signal $R(t)$. SPW-Rs were defined as events where $R(t)$ remained above 2 for 30 ms to 100 ms, and peaked at >5.

To detect delta waves, the LFP recorded in the mPFC was filtered (0–6 Hz) and z-scored, yielding $D(t)$. We extracted sequences ($t_{beginning}$, t_{peak}, t_{end}) of upward-downward-upward zero-crossings of $D'(t)$, corresponding to the putative beginning, peak and end of delta waves, respectively. Sequences lasting less than 150 ms or more than 500 ms were discarded. Delta waves corresponded to epochs where $D(t_{peak}) > 2$, or $D(t_{peak}) > 1$ and $D(t_{end}) < -1.5$.

For spindle detection, the LFP recorded in the mPFC was band-pass filtered (9–17 Hz) and z-scored. The squared magnitude of its Hilbert transform was smoothed using a 100-ms Gaussian window, yielding $S(t)$. Spindles corresponded to epochs where $S(t)$ remained above 2.5 for more than 0.5 s, and peaked at >5. Events separated by less than 0.4 s were merged, and combined events lasting more than 3 s were discarded.

Delta-spindle sequences were defined as epochs where spindle peaks occurred between 100 ms and 1.3 s following delta peaks. SPW-R–delta sequences corresponded to epochs where delta peaks occurred between 50 ms and 250 ms following ripple peaks. SPW-R–delta-spindle sequences corresponded to the conjunction of these events. Delta–SPW-R sequences corresponded to occurrences of ripple peaks between 50 ms and 400 ms following delta peaks.

Only sleep epochs preceding the encoding phase and lasting more than 1,200 s were used for these analyses.

Sleep scoring. Sleep stages (SWS/rapid eye movment) were determined by automatic K-means clustering of the theta/delta ratio extracted from the power spectrograms during the episodes where the animal was immobile (linear velocity <3 cm s^{-1} for at least 30 s, with brief movements <0.5 s).

Down states. Down states were defined as delta-wave centered epochs lasting 100–300 ms containing a maximum of three spikes. Only sessions with $n_{\text{PFC neurons}} > 7$ (average number of mPFC cells = 19, range 7–31) were used for down state detection and subsequent cross-correlation with delta waves.

Network activity during up-state transitions. For each cell, the activation latency was measured as its mean spike time within 200 ms of up state onset[29]. To compare PETHs triggered by up state transitions following induced versus endogenous, non-ripple-coupled delta waves, we computed the similarity index (PETH uniqueness) for each neuron as described previously[29]. Briefly, for each pair of neurons i and j, we computed the Euclidean distance d_{ij} between the PETH of i in endogenous up states, and the PETH of j in induced up states. The similarity index of neuron i is the proportion of neurons j for which $d_{ii} < d_{ij}$. Thus, a neuron with a similarity index greater than 0.5 has PETH features remaining consistent across endogenous and induced up states that can differentiate it from more than half of the other neurons. Bimodality in similarity index distributions was assessed using Hartigan's dip test on smoothed bootstrapped (n = 10,000) similarity indices[35].

Object responsivity. The arena was divided into four quadrants, two of which contained the objects. Distributions of firing rates in the empty quadrants were first estimated for each cell. Briefly, a random number of non-overlapping epochs of random durations were selected, adding up to 50% of the total time spent in the empty quadrants. This constituted one 'sample' over which the firing rate was computed. The procedure was repeated 1,000 times, yielding an estimated distribution F of firing rates in the empty quadrants. The responsivity index R to a given object was defined as the mean firing rate r over the corresponding quadrant, z-scored relative to F; that is, $R = (r - \mu)/\sigma$ where μ and σ are the mean and s.d. of F. Thus, the object responsivity index R measured by how much, relative to its baseline variability, a cell increased its firing rate around the object. Because inevitable micro-movements of the independently movable electrodes precluded reliable tracking of single cells over successive days, comparisons between the encoding and recall phases were performed at the population level.

Histology. At the end of the experiments, electrolytic lesions were made at the tip of the electrodes to verify their precise location (CA1 pyramidal layer and deep layers of the prelimbic mPFC). Rats were deeply anesthetized with a lethal dose of pentobarbital, and intracardially perfused with saline (0.9%, wt/vol) followed by 400 ml of paraformaldehyde (10%, wt/vol). Brains were then sliced into coronal sections (40 µm) and stained with cresyl-violet.

Data availability. The data that support the findings of this study are available from the corresponding author upon request.

A **Supplementary Methods Checklist** is available.

33. Hazan, L., Zugaro, M. & Buzsáki, G. Klusters, NeuroScope, NDManager: a free software suite for neurophysiological data processing and visualization. *J. Neurosci. Methods* **155**, 207–216 (2006).
34. Barthó, P. *et al.* Characterization of neocortical principal cells and interneurons by network interactions and extracellular features. *J. Neurophysiol.* **92**, 600–608 (2004).
35. Hartigan, J. & Hartigan, P. The dip test of unimodality. *Ann. Stat.* **13**, 70–84 (1985).

doi:10.1038/nn.4304